

Balancing Passive and Active Targeting to Different Tumor Compartments Using Riboflavin-Functionalized Polymeric Nanocarriers

Yoanna Tsvetkova,^{*,†,◆} Nataliia Beztsinna,^{‡,^,◆} Maike Baues,[†] Dionne Klein,^{†,§} Anne Rix,[†] Susanne K. Golombek,[†] Wa'el Al Rawashdeh,^{†,||} Felix Gremse,[†] Matthias Barz,[⊥] Kaloian Koynov,[#] Srinivas Banala,^{†,▽} Wiltrud Lederle,[†] Twan Lammers,^{†,○,Ⓟ} and Fabian Kiessling^{*,†,Ⓟ}

[†]Institute for Experimental Molecular Imaging, University Hospital and Helmholtz Institute for Biomedical Engineering, RWTH Aachen, Pauwelsstrasse 30, 52074 Aachen, Germany

[‡]Institute of Chemistry and Biology of Membranes and Nano-objects, CBMN UMR 5248, Bordeaux University, 33608 Pessac, France

[^]Department of Pharmaceutics, UIPS, Utrecht University, Universiteitsweg 99, 3584 CG Utrecht, The Netherlands

[§]Institute for Molecular Cardiovascular Research IMCAR, RWTH Aachen, Pauwelsstrasse 30, 52074 Aachen, Germany

^{||}Miltenyi Biotec GmbH, Friedrich-Ebert-Strasse 68, 51429 Bergisch Gladbach, Germany

[⊥]Institute of Organic Chemistry, Johannes Gutenberg University Mainz, Duesbergweg 10-14, 55099 Mainz, Germany

[#]Max Planck Institute for Polymer Research, Ackermannweg 10, 55128 Mainz, Germany

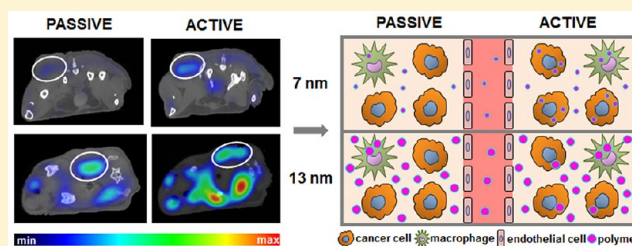
[▽]Institute of Organic Chemistry, RWTH Aachen, Landoltweg 1, 52074 Aachen, Germany

[○]Department of Targeted Therapeutics, University of Twente, P.O. Box 217, 750 AE Enschede, The Netherlands

Supporting Information

ABSTRACT: Riboflavin transporters (RFTs) and the riboflavin carrier protein (RCP) are highly upregulated in many tumor cells, tumor stem cells, and tumor neovasculature, which makes them attractive targets for nanomedicines. Addressing cells in different tumor compartments requires drug carriers, which are not only able to accumulate via the EPR effect but also to extravasate, target specific cell populations, and get internalized by cells. Reasoning that antibodies are among the most efficient targeting systems developed by nature, we consider their size (~10–15 nm) to be ideal for balancing passive and active tumor targeting. Therefore, small, short-circulating (10 kDa, ~7 nm, $t_{1/2} \sim 1$ h) and larger, longer-circulating (40 kDa, ~13 nm, $t_{1/2} \sim 13$ h) riboflavin-targeted branched PEG polymers were synthesized, and their biodistribution and target site accumulation were evaluated in mice bearing angiogenic squamous cell carcinoma (A431) and desmoplastic prostate cancer (PC3) xenografts. The tumor accumulation of the 10 kDa PEG was characterized by rapid intercompartmental exchange and significantly improved upon active targeting with riboflavin (RF). The 40 kDa PEG accumulated in tumors four times more efficiently than the small polymer, but its accumulation did not profit from active RF-targeting. However, RF-targeting enhanced the cellular internalization in both tumor models and for both polymer sizes. Interestingly, the nanocarriers' cell-uptake in tumors was not directly correlated with the extent of accumulation. For example, in both tumor models the small RF-PEG accumulated much less strongly than the large passively targeted PEG but showed significantly higher intracellular amounts 24 h after iv administration. Additionally, the size of the polymer determined its preferential uptake by different tumor cell compartments: the 10 kDa RF-PEGs most efficiently targeted cancer cells, whereas the highest uptake of the 40 kDa RF-PEGs was observed in tumor-associated macrophages. These findings imply that drug carriers with sizes in the range of therapeutic antibodies show balanced properties with respect to passive accumulation, tissue penetration, and active targeting. Besides highlighting the potential of RF-mediated (cancer) cell targeting, we show that strong tumor accumulation does not automatically mean high cellular uptake and that the nanocarriers' size plays a critical role in cell- and compartment-specific drug targeting.

KEYWORDS: Riboflavin, branched PEG, passive and active tumor targeting



Cancer therapies increasingly involve the administration of nanomedicines, which passively accumulate in malignant lesions due to enhanced permeability and retention (EPR) effect. Passive drug accumulation in tumors relies on highly fenestrated neovasculature and insufficient lymphatic and venous drainage.^{1–3} Nanomedicine delivery based on EPR,

however, has limitations. EPR varies significantly not only across different tumor types but also within different subregions

Received: March 19, 2017

Revised: June 22, 2017

Published: July 17, 2017



of a single tumor.^{1,4,5} Furthermore, a dense fibrotic micro-environment can lead to poor diffusion of the nanomedicines and therefore may hinder their deep penetration. Thus, depending on their size and surface properties, many drug carriers such as nanoparticles, micelles, or liposomes tend to accumulate in the perivascular space of tumors and fail to reach the cancer cells.^{6–8} Active targeting is often suggested to improve nanomedicine accumulation, because it may increase the retention of nanocarriers through specific cellular uptake. This, however, is only possible if sufficient passive accumulation occurs, if the size of nanomedicines allows for deep tissue penetration and if the target is accessible. Therefore, it is still an open question how nanomedicine accumulation in tumors can be maximized and how passive and active targeting mechanisms need to be balanced. Furthermore, enhanced nanomedicine accumulation does not automatically indicate higher therapeutic efficacy. Homogeneous drug distribution within the tumor, as well as balanced delivery to all relevant tumor compartments with optimized uptake by cancer cells, cancer stem cells, endothelium, and stroma will have a significant impact on the therapeutic outcome.

In order to better understand how passive and active tumor accumulation and cellular uptake are influenced by the size of a nanocarrier, we employed two differently sized branched polyethylene glycol (PEG) polymers, which have clearly different pharmacokinetic profiles in terms of plasma residence and volume of distribution.⁹ We evaluated their pharmacokinetics, biodistribution, and cell-uptake in two different tumor models by using noninvasive combined computed tomography and fluorescence molecular tomography (CT/FMT)^{10,11} and fluorescence microscopy (Figure 1).

The small polymer (10 kDa, $D_H \sim 7$ nm) has a relatively short blood half-life, and therefore is expected to display low

EPR effect in cancer lesions. The larger branched PEG polymer (40 kDa, $D_H \sim 13$ nm) is just above the renal threshold, and thus has a significantly longer blood half-life, likely leading to much more pronounced EPR-mediated tumor accumulation. Furthermore, with a size of approximately 13 nm, the 40 kDa polymer is within the size range of IgG antibodies ($D_H \sim 10–15$ nm).^{12,13} Antibodies are among the most potent targeting systems developed by nature and we hypothesize that their good performance is supported by the evolutionary development of an ideal size. There are different types of antibodies: IgM antibodies ($D_H \sim 30$ nm) are larger, have more binding sites, and are responsible for early inflammation phases and mostly bind antigens in the blood. Thus, their size may be evolutionarily optimized for retention in systemic circulation and not for targeting areas far away from blood vessels.¹⁴ In contrast, the smaller IgG antibodies extravasate strongly in tissues, predominantly in areas of inflammation or cancer, where inflammatory and angiogenic factors increase vascular permeability.^{10,14} On the basis of this notion, we hypothesize that nanomedicines in the size range of IgG may offer an optimal balance between a sufficiently long blood half-life, passive accumulation at pathological sites, and deep penetration into tissues and thus enable efficient targeting of extravascular epitopes. Because smaller antibody formats, such as single chain antibodies and nanobodies, have also shown excellent extravascular targeting capability despite their shorter blood half-life, we decided to evaluate both 7 and 13 nm large polymeric nanocarriers with respect to their potential for drug delivery to different tumor compartments.

We selected riboflavin (RF) as a targeting ligand since its metabolism is shown to be highly upregulated in cancer cells, cancer stem cells and cells of the tumor microenvironment.^{15–18} The cellular uptake of RF (vitamin B2), similarly to folic acid (vitamin B9), is facilitated by high-affinity receptor-mediated endocytosis: transmembrane transporters (RFTs) and carrier protein (RCP) that are overexpressed by many cancer cells and allow for tumor-specific drug delivery of RF-targeted nanomedicines.¹⁹ As model nanocarriers, we employed two four-arm PEG polymers labeled with the fluorescent dye cyanine 5.5 (Cy5.5) on one arm in order to enable their detection by CT/FMT. We used the RF-derivative carboxymethylriboflavin²⁰ as a targeting moiety and conjugated it to the residual three arms. All polymer conjugates were purified on reversed-phase HPLC and the chemical modification was monitored with UV/vis spectroscopy. As shown in Figure 2, the polymers, functionalized with both RF and Cy5.5, displayed an absorption spectrum that is characteristic for both conjugated molecules (strong absorption peaks of RF at 260 and 370 nm in the UV range and a maximum at 450 nm in the visible range, along with a strong absorption peak of the cyanine dye at 680 nm). As expected, only the absorption spectrum of the fluorescent dye was found in the RF-free control polymer. The purity and the hydrodynamic diameter (D_H) of the polymers were measured with fluorescence correlation spectroscopy (FCS) in PBS buffer. The 10 kDa PEG displayed $D_H \sim 7$ nm, and the D_H of the 40 kDa PEG was measured to be approximately 13 nm. In addition, the polymers' properties in terms of size and selective binding to RCP were also analyzed in biological media (plasma and serum). The results (Supporting Information, Figures S2 and S3) show that there was no protein adsorption on the polymeric nanocarriers and the RF-PEGs retained their targeting efficacy in serum.

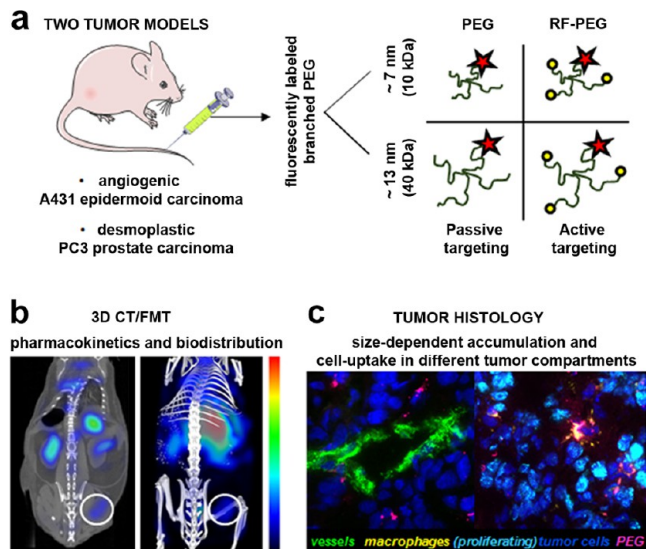


Figure 1. Schematic overview of the study. (a) Differently sized polymers were administered *in vivo* in mice bearing epidermoid carcinoma (A431) and prostate carcinoma (PC3) xenografts. (b) The polymers' pharmacokinetics and biodistribution were assessed *in vivo* using CT/FMT. (c) Polymers' accumulation in tumors and uptake by cells of different tumor compartments were evaluated histologically. Clip art was used from the Servier's "Medical Art" database (<http://www.servier.com/Powerpoint-image-bank>) and modified.

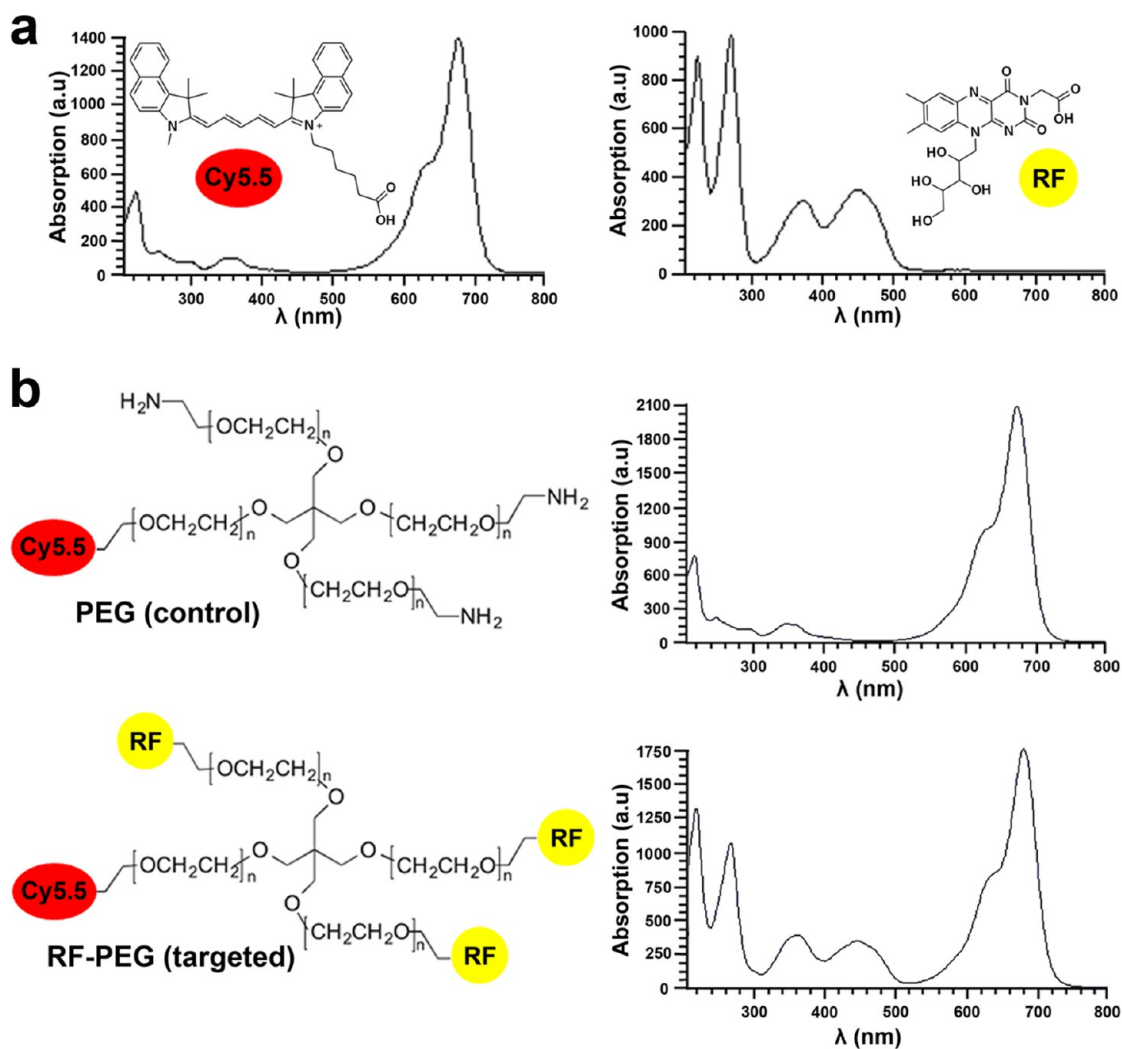


Figure 2. Scheme illustrating the composition of the polymeric nanocarriers and absorption spectra of the near-infrared dye Cy5.5, RF-derivative, and labeled polymers. (a) Absorption spectra of Cy5.5 (left) and RF derivative (right). (b) Branched PEGs labeled with Cy5.5 (PEG), and with RF-derivative and Cy5.5 (RF-PEG) are shown on the left. The corresponding absorption spectra of the labeled polymers are presented on the right.

The cellular uptake of the 10 and 40 kDa targeted and nontargeted polymers was tested in A431 squamous cell carcinoma and PC3 prostate cancer cells, which are both known to display high RF uptake.¹⁸ Polymer internalization was evaluated by fluorescence microscopy at excitation wavelength of 680 nm and showed up to three times higher cellular uptake for the targeted than for nontargeted PEG (Figure 3). Blocking RFTs by the addition of a 20-fold excess of targeted polymers, not labeled with Cy5.5, reduced the cellular uptake of RF-PEG to the levels of nontargeted PEG, confirming its specific receptor-mediated internalization. The uptake ratios of targeted and nontargeted 10 and 40 kDa PEGs were similar. Overall, however, the larger polymers were internalized by the cells to a lower extent (Figure 3b), which is likely due to the larger size, leading to a slower internalization. Furthermore, the cellular uptake of the polymers was evaluated at 4 °C. The results showed a significant decrease ($p < 0.05$) in polymer internalization that indicated that the uptake of the nanocarriers is mediated through energy-dependent endocytosis. In line with these results on cancer cells, mouse macrophages also showed an enhanced uptake of RF-targeted PEG that could be competitively blocked and reduced by decreasing the

temperature to 4 °C. However, since these cells already show a relatively high unspecific phagocytic uptake of the polymers, the differences were smaller than for the cancer cells (Supporting Information, Figure S4).

Evaluation of the Pharmacokinetics and Biodistribution of PEG and RF-PEG in Vivo. The polymeric nanocarriers were administered intravenously to CD1 nude mice bearing A431 and PC3 tumor xenografts. In order to determine the blood half-life of the differently sized PEGs, blood samples were collected from each animal at different time points and evaluated with 2D fluorescence reflectance imaging (FRI). The glomerular permeability threshold for linear PEG polymers is reported to be approximately 30 kDa.²¹ Thus, it was expected that the 40 kDa branched PEG would remain in the blood circulation for significantly longer time compared with its 10 kDa counterpart. Indeed, blood half-life of approximately 1 h for the 10 kDa and 13 h for the 40 kDa PEG were obtained when fitting the decreasing fluorescence intensity of the polymers in blood over time (Figure 4a) as an exponential decay curve (Figure 4b). Functionalization of the polymers with RF did not significantly change their blood half-lives.

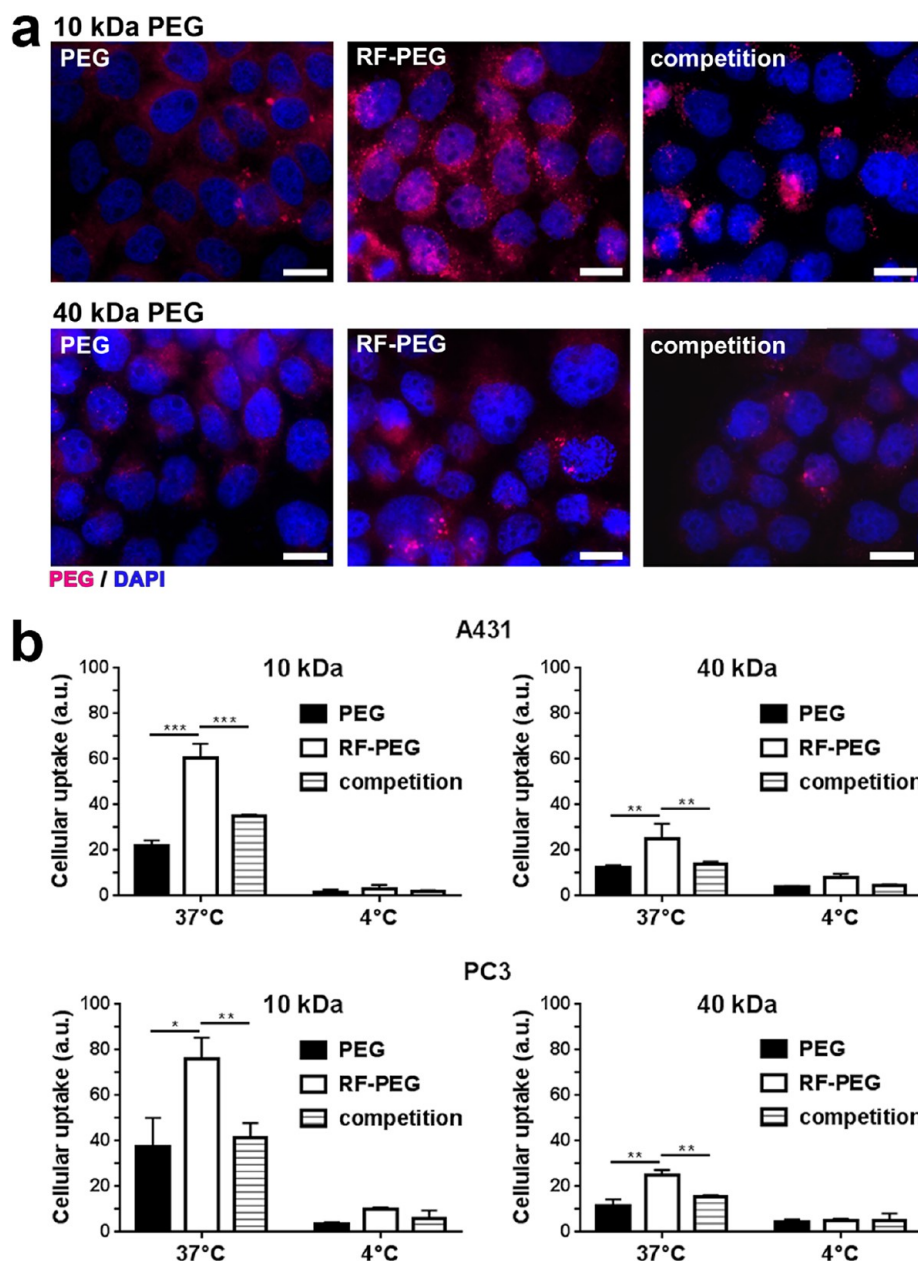


Figure 3. Representative fluorescence images and evaluation of cellular uptake of 10 and 40 kDa polymers. (a) (a) Fluorescence microscopy images of A431 cells after incubation at 37 °C with 10 and 40 kDa polymers (red) are in line with the quantification and show RF-PEGs in a perinuclear location which is in line with a lysosomal storage. Cell nuclei are counterstained with DAPI (blue). Scale bar: 15 μm . (b) The quantification of the cellular uptake at 37 °C of 10 kDa and 40 kDa PEGs based on fluorescence intensity measurements clearly shows a higher uptake of targeted versus nontargeted polymers in both cell lines and the significant reduction of cellular internalization after competitive receptor blockade. The cellular uptake was significantly decreased at 4 °C, which indicates an energy-dependent endocytosis. *, $p < 0.05$; **, $p < 0.01$; ***, $p < 0.001$.

In vivo CT/FMT quantification of the polymers' organ distribution in mice bearing A431 tumors is shown in Figure 5a and ex vivo data acquired by 2D FRI is presented in Figure 5b. Because of their lower molecular weight, the 10 kDa polymers showed a faster extravasation and penetration in the tissue than the larger polymers and were characterized by a lower retention in organs. In addition, 72 h after injection there was still a substantial amount of the 40 kDa polymers circulating in the blood that contributed to the measured amounts in the organs. In line with this, the amount of 10 kDa PEG in all organs, measured by in vivo

CT/FMT, was three times lower in comparison with the 40 kDa PEG 72 h after injection.

A higher fluorescence signal in the liver was measured for the 10 kDa targeted polymers compared to the 10 kDa control group ($7.2 \pm 0.4\% \text{ID}/\text{cm}^3$ vs $4.4 \pm 0.5\% \text{ID}/\text{cm}^3$, $p < 0.01$), which may be explained by RF-mediated macrophage uptake that complements the unspecific polymer phagocytosis. This difference was not prominent for the large polymer, most likely due to the much higher unspecific liver uptake of approximately $13.6 \pm 1.9\% \text{ID}/\text{cm}^3$ that, as in tumors, masks the actively bound and retained polymer fraction. In all other

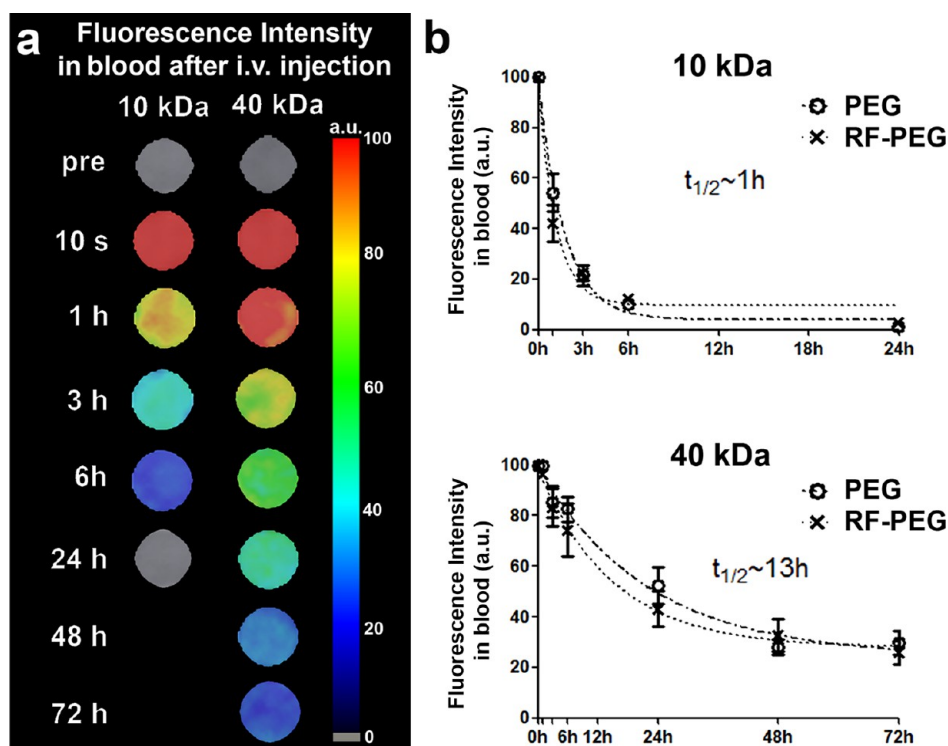


Figure 4. Blood half-life of 10 and 40 kDa branched PEGs in A431 tumor model. (a) Fluorescence intensity of blood samples measured with 2D FRI after iv injection of 10 kDa and 40 kDa Cy5.5-labeled RF-targeted and control polymers. (b) Plot of the blood fluorescence intensity at different time points to assess the blood half-lives of the polymers. There is no significant difference in the blood half-lives of RF-targeted and control polymers ($n = 5$). As expected, the blood half-lives of the 10 kDa polymers are much shorter than of the 40 kDa PEGs.

organs, there was no significant increase in polymer uptake upon functionalization with RF. Similar values were obtained for the mice bearing PC3 xenografts (Supporting Information, Table S1).

CT/FMT measurements, performed during the initial distribution phase of the 10 kDa polymers at 15 min after intravenous (iv) administration, revealed no significant difference between the amount of control and targeted polymers in the tumors (Figure 6a). However, this does not necessarily mean that there was no early binding of the 10 kDa RF-PEGs. Small polymers show a fast extravasation and tissue penetration, which leads to a rapid and strong enhancement of their concentration in the extravascular space shortly after iv injection, masking the fraction of target-bound polymers. Subsequently, small polymers redistribute into circulation, and as the amount of the carriers in the blood rapidly decreases, the retention of actively targeted probes in the tumor becomes more pronounced. This explains the fact that 3 h after administration, when 80% of the injected polymers were cleared from the blood, the difference between passive and active targeting started to become prominent. Significant differences were observed 6 and 24 h post injection, when most unbound polymers have re-entered circulation and were subsequently cleared from the blood. The amount of the 10 kDa polymers accumulated in the tumor lesion, quantified *in vivo* 24 h after PEG administration, was up to twice as high for the targeted as for the control probe in A431 (1.3 ± 0.2 vs $0.6 \pm 0.1\%ID/cm^3$, $p < 0.05$) and 30% higher in PC3 tumors (0.6 ± 0.1 vs $0.4 \pm 0.1\%ID/cm^3$, $p < 0.05$) (Figure 6).

A significantly different time profile of tumor accumulation was observed for the 40 kDa polymers. In contrast to the small polymers, which have a large volume of distribution at early

time points and undergo rapid renal elimination, the larger nanocarriers exhibited continuous tumor accumulation over 24 h. The accumulation of 40 kDa polymers in tumors was strongly mediated via EPR, and their concentration in the cancerous lesions was approximately four times higher than that of the small polymers (in A431 tumors, RF-PEGs, $4.6 \pm 0.6\%ID/cm^3$ (40 kDa) vs $1.3 \pm 0.2\%ID/cm^3$ (10 kDa); PEGs, $4.7 \pm 1.1\%ID/cm^3$ (40 kDa) vs $0.6 \pm 0.1\%ID/cm^3$ (10 kDa)). In PC3 tumors, RF-PEGs, $2.6 \pm 0.4\%ID/cm^3$ (40 kDa) vs $0.6 \pm 0.1\%ID/cm^3$ (10 kDa); PEGs, $2.6 \pm 0.3\%ID/cm^3$ (40 kDa) vs $0.4 \pm 0.1\%ID/cm^3$ (10 kDa)). Interestingly, however, there was no significant difference between the amount of the 40 kDa RF-PEGs and PEGs in both tumor models up to 72 h after injection (Figure 6b). This may be due to the high polymer amount passively accumulated in the tumor, which renders active retention insignificant.

These data indicate that active targeting only improves the tumor accumulation of small nanocarriers if these have short blood half-life, fast compartment exchange, and low tissue retention. As the size of the probe increases, such as in the case of the 40 kDa polymers, EPR becomes prominent and enhances the overall nanoparticles accumulation. Because under these circumstances strong tissue retention is given, the effect of active targeting on tumor accumulation becomes less pronounced and may not be detectable.

Although the tendency in polymers' longitudinal accumulation was similar for both tumor models, there was a clear difference between the overall amount of PEGs in the A431 and the PC3 xenograft. The area below the accumulation-time curves of the control polymers showed that A431 tumors generally accumulated higher amounts of the nanocarriers (Figure 7a). Since collagen is one of

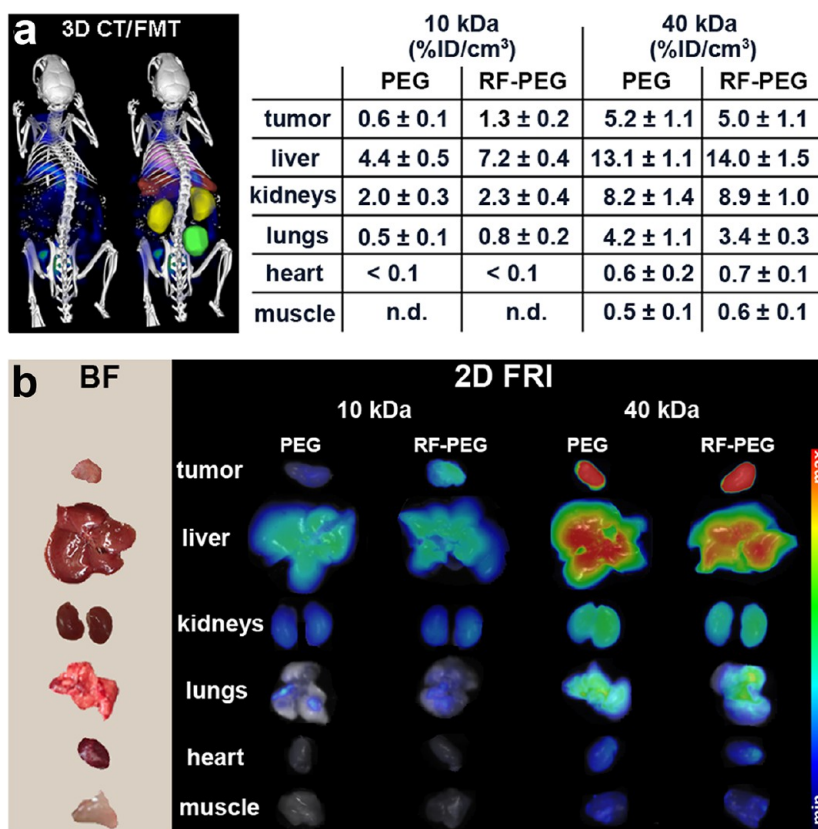


Figure 5. Biodistribution of fluorescently labeled 10 kDa PEGs 24h post iv injection, and 40 kDa PEGs 72 h post iv injection in mice bearing A431 tumors quantified by 3D CT/FMT. (a) An example of a fused CT/FMT image of a mouse with organ segmentation is shown on the left. The results of the 3D CT/FMT quantification of polymer amounts in the organs is presented as percentage of the injected dose per cm³ (right). Please note that despite higher amounts of the 40 kDa in the organs, compared with the 10 kDa probe, tumor-to-liver ratios are higher for the larger PEGs. In addition, it needs to be considered that the data was acquired when significant amounts of the 40 kDa polymer were still in the blood circulation. (b) Ex vivo bright-field (BF) organ images (left) and their corresponding 2D FR images indicating the accumulation of the fluorescently labeled PEGs (right).

the major determinants of interstitial transport and thus of accumulation of nanocarriers in the interstitial space,²² we analyzed the collagen density and the vascularity of both xenografts by two-photon microscopy in order to explain the difference in the polymers' extravasation. In two-photon microscopy, the vessel segmentation is based on the injection of fluorescently labeled lectin, which stains only the blood perfused vessels. Additionally, second harmonic generation enables the visualization of stromal collagen and collagen volume fraction analysis. Evaluation of tumor cryosections indicated almost three times fewer (functional) vessels and a 7-fold higher collagen density for the PC3 model (Figure 7b). Thus, the lower blood supply and denser fibrotic network may be the driving factors explaining the lower polymer diffusion and distribution within the tumor and explain the lower amount of PEG accumulation in the PC3 xenograft compared to the A431 model.

Although passive tumor accumulation via EPR is the dominant mechanism of action for nanomedicines with size above the renal elimination threshold, it does not entail efficient intracellular drug delivery. Passively targeted nanocarriers usually release their drug payload in the extracellular matrix, which is often sufficient.²³ Some drugs, however, cannot diffuse efficiently and do not reach the tumor cells. Also for highly toxic substances, intracellular release from the drug delivery system is desirable. Thus, the use of solely passively targeted drug delivery systems for which the cellular uptake relies on

nonspecific endocytosis, may not always be efficient.²⁴ Therefore, to achieve high therapeutic efficiency, it is necessary for many drugs and nanomedicines to not only passively accumulate in the tumor but also to actively trigger cellular internalization. In addition, the therapeutic efficiency will also be influenced by the cellular compartments that are predominantly targeted. In this context, different tumor types and drugs may require different adjustments of drug delivery to tumor or stromal cells, the latter including endothelial cells, macrophages, (myo-)fibroblasts and cancer cells.

Histological analysis of tumor cryosections was performed to evaluate the amount of accumulated and internalized polymers. Fluorescence microscopy of unfixed tumor tissue enabled the quantification of the whole accumulated polymer content in the extravascular extracellular space and within cells. In order to quantify only the amount of nanocarrier taken up by cells, the tumor sections were fixed and washed extensively to remove the noninternalized polymers. Representative fluorescence images of unfixed and fixed cryosections are shown in Figure 8a. The histological evaluation, presented in Figure 8b, showed that the amount of accumulated polymer could not be directly correlated with the amount of polymer internalized by cells. In line with the in vivo CT/FMT data, the histological analysis revealed no difference in the overall tumor accumulation between 40 kDa RF-PEG and PEG in both A431 and PC3 xenografts. However, in terms of cellular uptake, the 40 kDa RF-PEG showed significantly higher internalization vs their

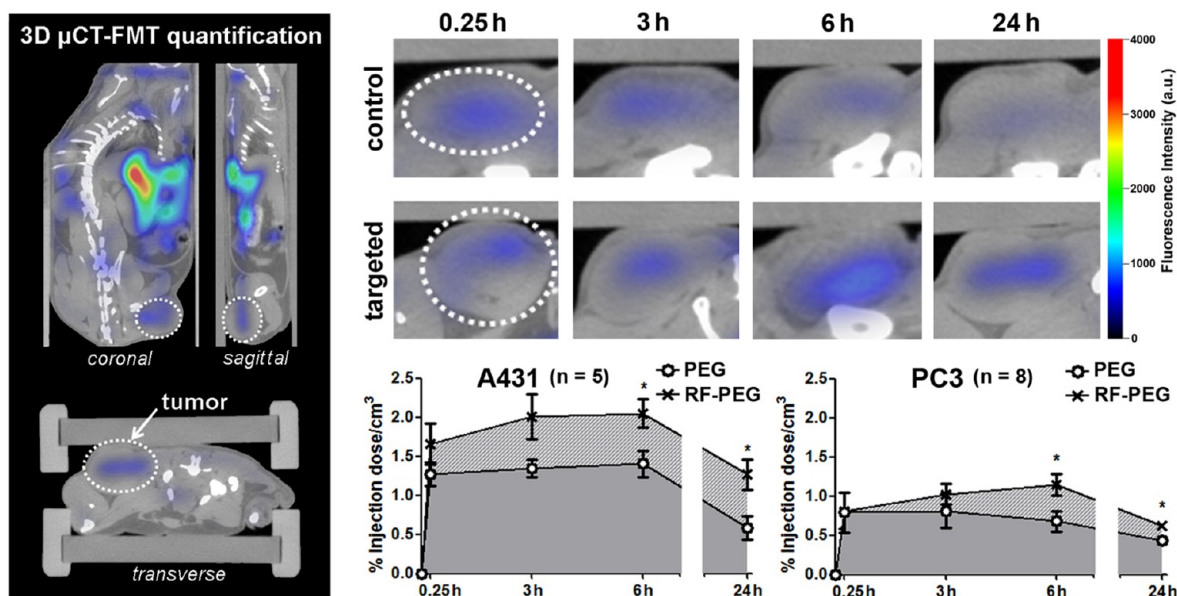
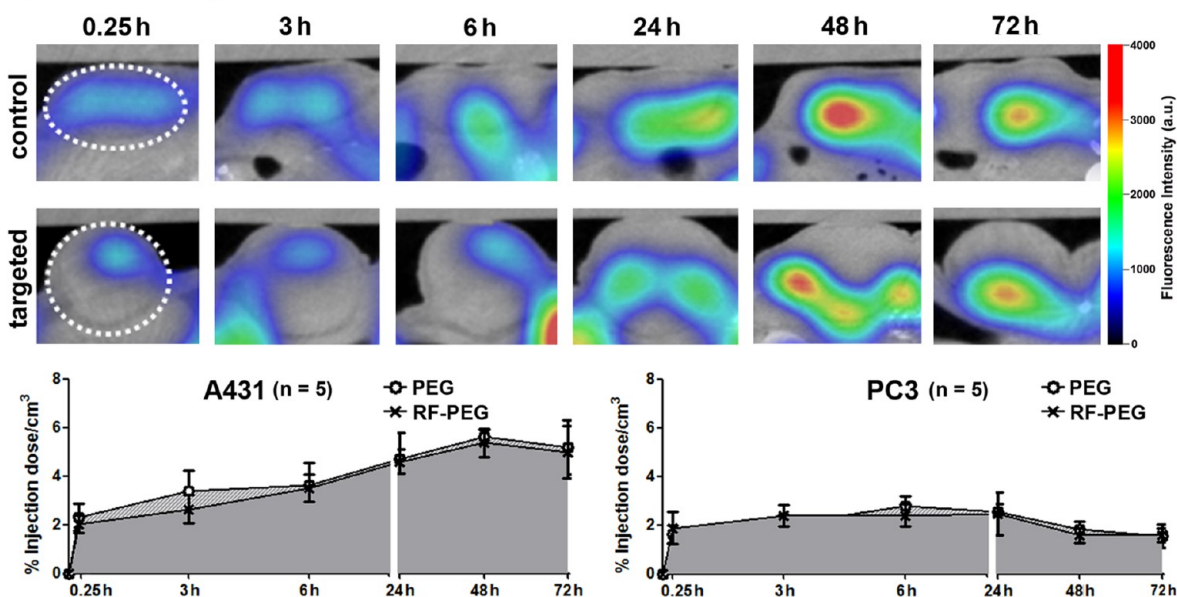
a 10 kDa PEG tumor accumulation**b** 40 kDa PEG tumor accumulation

Figure 6. Representative CT/FMT images of A431 tumors at different time points after iv injection of targeted and control 10 kDa (a) and 40 kDa (b) polymers and plots indicating their accumulation in A431 and PC3 tumor xenografts. Active targeting improved tumor accumulation only for the 10 kDa probe, which is true for both the highly angiogenic A431 and the desmoplastic PC3 tumors. In addition, the differences in the dynamics of 10 kDa and 40 kDa polymer accumulation are clearly demonstrated.

passively targeted counterparts: 2.5 ± 0.3 vs 1.7 ± 0.1 fluorescence intensity (a.u.), $p < 0.05$ in A431 tumors, and 1.6 ± 0.3 vs 0.5 ± 0.1 fluorescence intensity (a.u.), $p < 0.01$ in PC3 tumors, respectively. The difference between accumulation and internalization is even more pronounced when comparing the 40 kDa nontargeted polymers with the small RF-PEGs. Although the 10 kDa RF-PEG accumulated to much lower extent than the nontargeted 40 kDa PEG, its cellular uptake was found to be nearly three times higher (3.8 ± 0.9 vs 1.6 ± 0.1 fluorescence intensity (a.u.) $p < 0.05$ in A431 tumors and 1.4 ± 0.2 vs 0.5 ± 0.1 fluorescence intensity (a.u.), $p < 0.01$ in PC3 tumors). This data

suggests that the control polymers accumulated predominantly in the extracellular compartment with low degree of nonspecific cellular uptake, whereas the RF-PEGs were retained intracellularly.

The next important question was to characterize the cellular compartments that internalized the polymers and to investigate whether nanocarriers' size or RF-targeting changed the preferential uptake of certain cell types. For this purpose, immunohistochemical stainings were performed: anti-CD68 and anti-Ki67 antibodies were used to mark macrophages and proliferating cells and their colocalization

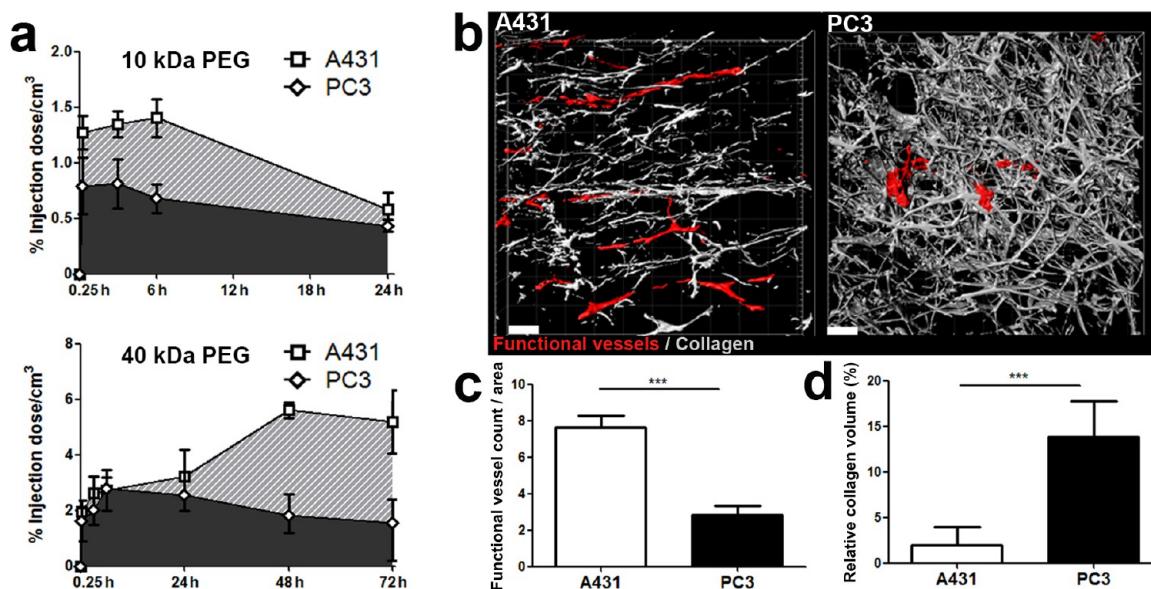


Figure 7. Tumor properties and perfusion with nanocarriers. (a) Plots demonstrate that the accumulation of 10 and 40 kDa control polymers was substantially lower in PC3 than A431 tumors. (b) The three-dimensional (3D) surface-rendered view of representative two-photon images for both tumor models, A431 and PC3, showing blood vessels and collagen density. (c) Quantification of vessel density. (d) Quantification of collagen content indicates the desmoplastic nature and lower vascularization of the PC3 tumors, which may explain the lower accumulation of the polymers. Scale bar: 50 μm .

with the polymers' signal is shown in Figure 8c. Blood vessel endothelial cells were stained with anti-CD31 antibodies, and DAPI was used to mark the cell nuclei. Histological analysis, presented in Figure 8d, shows that the presence of the targeting ligand and the size of the nanocarrier account for a preferential uptake in different tumor compartments. In general, nontargeted polymers were taken up in only low amounts by all cell types. However, there were differences in the cellular preference between the 10 kDa and 40 kDa polymers. While 10 kDa PEGs were mostly found in tumor cells, followed by macrophages and endothelial cells, the 40 kDa PEGs showed highest affinity to macrophages, followed by tumor cells and only negligible uptake by the endothelium. This may be due to the high concentration and long retention of the large polymers in the extravascular, extracellular space (EES), and their slower penetration/diffusion into tissue (Supporting Information, Figure S5) and thus, stronger exposure to interstitial stroma than to cancer cells. Higher macrophage-uptake, however, does not mean that 40 kDa RF-PEG would be a less effective drug carrier. Tumor-associated macrophages have been described to act as a slow-release reservoir of nanotherapeutics and may transfer them to neighboring tumor cells.²⁵ Furthermore, eradicating M2-type tumor macrophages has been reported to strongly reduce cancer cell invasion and metastasis.²⁶ In addition, there was still a significant amount of free 40 kDa RF-PEG in the interstitial space of the tumor tissue 72 h p.i., which over time may diffuse and get internalized by the tumor cells.

Interestingly, for the 40 kDa polymer, there was a tendency for a smaller difference between macrophage- and tumor cell-uptake upon conjugation with RF (Figure 8d). This likely results from the higher impact of active targeting on tumor cells than on macrophages with the latter already internalizing significant amounts of the polymer by unspecific phagocytosis, while tumor cells show hardly any RF-independent uptake. For the deeper understanding of underlying processes of tumor accumulation and

compartmentalization intravital microscopy could be employed in future studies to provide time-resolved high-definition images of polymer diffusion and uptake in vascular, cancer, stromal, and immune cells.^{27,28}

Active targeting with RF significantly enhanced the uptake of both polymers without strongly changing their cell compartmental preferences. The uptake of 7–13 nm sized (RF-targeted) PEG polymers by endothelial cells was found to be low. This is not in line with previous findings on ~ 100 nm sized riboflavin-labeled USPIO nanoparticles,^{16,17} which were mainly localized in endothelial cells and macrophages. Either endothelial cells internalize PEG less preferentially than USPIO nanoparticles or, more likely, the lower endothelial uptake is only relative and can be explained by the fact that riboflavin-functionalized USPIO with their considerably larger size and short blood half-life did not efficiently penetrate into tumor tissue and showed markedly lower uptake by macrophages and hardly any uptake by tumor cells.

In summary, besides supporting the use of riboflavin as an interesting target for cancer nanomedicines, this study highlights important links between nanomedicine size and passive and active targeting mechanisms. We show that active targeting only improves the accumulation of polymeric nanocarriers if there is low baseline retention and if the EPR effect is not prominent. These properties, which are typical for very small polymers, are considered to be crucial for nanodiagnostics, which intend to highly specifically visualize the expression of molecular targets. We furthermore demonstrated that active targeting with riboflavin strongly improves cellular uptake of both small and large polymers by cancer cells, macrophages, and proliferating cells and that even small differences in nanocarrier size have an impact on cellular compartmentalization (overview presented in Figure 9). In this context, we hypothesize that for therapeutic applications targeted nanocarriers with size dimensions in the range of IgG antibodies have the ideal size to circulate long, selectively

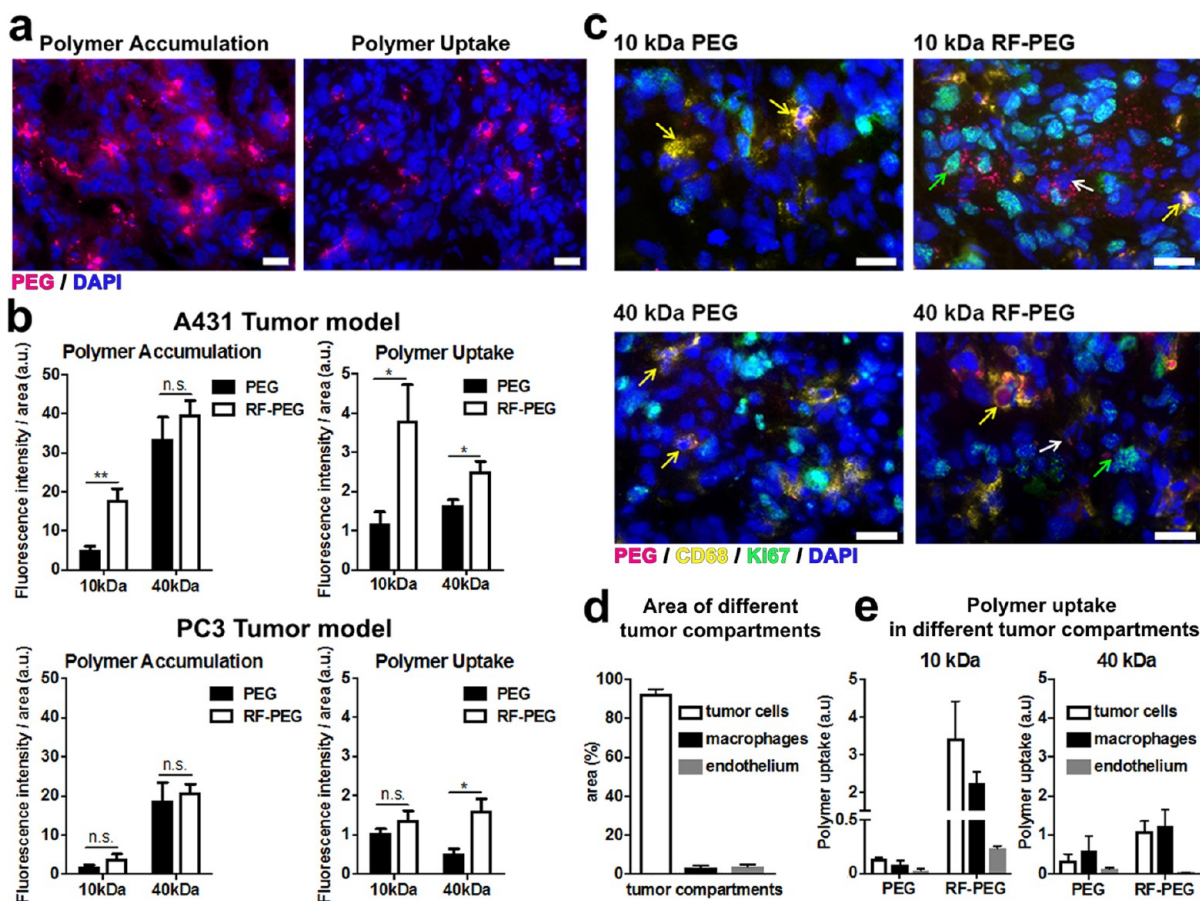


Figure 8. Histological analysis performed 24 h after iv injection of 10 kDa polymers and 72 h after iv injection of 40 kDa polymers. (a) Representative images of an unfixed cryosection (left), showing the amount of accumulated polymers, and a fixed and washed cryosection (right), showing the amount of internalized polymers, for 10 kDa RF-PEG in A431 tumor model. Scale bar: 20 μm . (b) Histological quantification of nanocarriers' total tumor accumulation (left) and intracellular accumulation (right) based on fluorescence intensity measurements of A431 and PC3 tumor cryosections. In both tumor models, there was a higher passive accumulation of 40 kDa than 10 kDa polymers. Active targeting improved the accumulation of the small polymers but hardly had any effect on the accumulation of the 40 kDa polymers. However, for both tumor models cellular internalization was strongly improved by active targeting. Please note that in particular in the highly angiogenic A431 tumor model, tumor accumulation did not match cellular internalization. *, $p < 0.05$; **, $p < 0.01$; n.s., not significant. (c) Fluorescence images illustrating the cellular uptake of the 10 kDa and 40 kDa polymers in A431 tumors. PEG is shown in red, macrophages (CD68) in yellow, proliferating cells (Ki67) in green, and cell nuclei (DAPI) in blue. Arrows show polymer accumulation in different cell types (white arrows for tumor cells, yellow arrows for macrophages, green arrows for proliferating cells). There was only a low uptake of passively targeted 10 kDa and 40 kDa polymers, predominantly by tumor macrophages. The cell-uptake of the RF-PEGs was much more pronounced. Scale bar: 20 μm . (d) Histological evaluation of the area percentage of different tumor compartments: cancer cells make up approximately 90% of the total tumor area, while macrophages and endothelium occupy only about 5%. (e) Histological evaluation of polymer uptake in different cell compartments. 10 kDa RF-PEG was predominantly located in (proliferating) tumor cells, 40 kDa RF-PEG was most strongly internalized by macrophages.

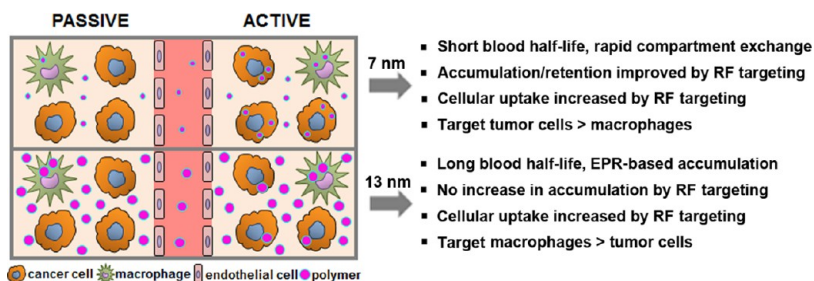


Figure 9. Overview of polymers' in vivo performance with respect to tumor accumulation and cellular uptake based on size and targeting ligand.

extravasate in tissues with increased vascular permeability, passively accumulate in these tissues via EPR, penetrate deeply, effectively find their extravascular targets, and localize to the intended cellular compartments.

■ ASSOCIATED CONTENT

📄 Supporting Information

The Supporting Information is available free of charge on the ACS Publications website at DOI: 10.1021/acs.nanolett.7b01171.

Materials and methods for the synthesis and characterization of the polymeric conjugates, nanocarriers' uptake, selective binding study, and histological analysis (PDF)

AUTHOR INFORMATION

Corresponding Authors

*E-mail: (Y.T.) yoanna.tsvetkova@gmail.com.

*E-mail: (F.K.) fkiessling@ukaachen.de.

ORCID

Twan Lammers: 0000-0002-1090-6805

Fabian Kiessling: 0000-0002-7341-0399

Author Contributions

◆Y.T. and N.B. contributed equally to the work.

Notes

The authors declare no competing financial interest.

ACKNOWLEDGMENTS

We thank Benjamin Theek for providing useful tools for the histological tumor evaluation. We also gratefully acknowledge the financial support by the German Research Foundation (DFG: SFB1066-1/-2) and by the Helmholtz Society Portfolio grant "Technologie und Medizin – Multimodale Bildgebung zur Aufklärung". This work is also supported by the Two-Photon Imaging core facility at the Interdisciplinary Center for Clinical Research (IZKF) within the Faculty of Medicine at RWTH Aachen University.

REFERENCES

- (1) Maeda, H.; Wu, J.; Sawa, T.; Matsumura, Y.; Hori, K. *J. Controlled Release* **2000**, *65*, 271–284.
- (2) Heldin, C.-H.; Rubin, K.; Pietras, K.; Östman, A. *Nat. Rev. Cancer* **2004**, *4*, 806–813.
- (3) McDonald, D. M.; Baluk, P. *Cancer Res.* **2002**, *62*, 5381–5385.
- (4) Kunjachan, S.; Detappe, A.; Kumar, R.; Ireland, T.; Cameron, L.; Biancur, D. E.; Motto-Ros, V.; Sancey, L.; Sridhar, S.; Makrigiorgos, G. M.; Berbeco, R. I. *Nano Lett.* **2015**, *15*, 7488–7496.
- (5) Maeda, H.; Matsumura, Y. *Adv. Drug Delivery Rev.* **2011**, *63*, 129–130.
- (6) Jain, R. K. *Cancer Res.* **1987**, *47*, 3039–3051.
- (7) Barua, S.; Mitragotri, S. *Nano Today* **2014**, *9*, 223–243.
- (8) Kunjachan, S.; Pola, R.; Gremse, F.; Theek, B.; Ehling, J.; Moeckel, D.; Hermanns-Sachweh, B.; Pechar, M.; Ulbrich, K.; Hennink, W. E.; Storm, G.; Lederle, W.; Kiessling, F.; Lammers, T. *Nano Lett.* **2014**, *14*, 972–981.
- (9) Yamaoka, T.; Tabata, Y.; Ikada, Y. *J. Pharm. Sci.* **1994**, *83*, 601–606.
- (10) Gremse, F.; Theek, B.; Kunjachan, S.; Lederle, W.; Pardo, A.; Barth, S.; Lammers, T.; Naumann, U.; Kiessling, F. *Theranostics* **2014**, *4*, 960–971.
- (11) Kunjachan, S.; Gremse, F.; Theek, B.; Koczera, P.; Pola, R.; Pechar, M.; Etrych, T.; Ulbrich, K.; Storm, G.; Kiessling, F.; Lammers, T. *ACS Nano* **2013**, *7*, 252–262.
- (12) Radomsky, M. L.; Whaley, K. J.; Cone, R. A.; Saltzman, W. M. *Biomaterials* **1990**, *11*, 619–624.
- (13) Armstrong, J. K.; Wenby, R. B.; Meiselman, H. J.; Fisher, T. C. *Biophys. J.* **2004**, *87*, 4259–4270.
- (14) Charles A Janeway, J.; Travers, P.; Walport, M.; Shlomchik, M. J. *The distribution and functions of immunoglobulin isotypes*; New York: Garland Science; 2001.
- (15) Miranda-Lorenzo, I.; Dorado, J.; Lonardo, E.; Alcalá, S.; Serrano, A. G.; Clausell-Tormos, J.; Cioffi, M.; Megias, D.; Zagorac, S.; Balic, A.; Hidalgo, M.; Erkan, M.; Kleeff, J.; Scarpa, A.; Sainz, B., Jr; Heeschen, C. *Nat. Methods* **2014**, *11*, 1161–1169.
- (16) Jayapaul, J.; Arns, S.; Bunker, M.; Weiler, M.; Rutherford, S.; Comba, P.; Kiessling, F. *Nano Res.* **2016**, *9*, 1319–1333.

(17) Jayapaul, J.; Arns, S.; Lederle, W.; Lammers, T.; Comba, P.; Gätjens, J.; Kiessling, F. *Biomaterials* **2012**, *33*, 8822–8829.

(18) Beztzinna, N.; Tsvetkova, Y.; Bartneck, M.; Lammers, T.; Kiessling, F.; Bestel, I. *Bioconjugate Chem.* **2016**, *27*, 2048–2061.

(19) Beztzinna, N.; Solé, M.; Taib, N.; Bestel, I. *Biomaterials* **2016**, *80*, 121–133.

(20) Caelen, I.; Kalman, A.; Wahlström, L. *Anal. Chem.* **2004**, *76*, 137–143.

(21) Yamaoka, T.; Tabata, Y.; Ikada, Y. *J. Pharm. Sci.* **1994**, *83*, 601–606.

(22) Chauhan, V. P.; Stylianopoulos, T.; Boucher, Y.; Jain, R. K. *Annu. Rev. Chem. Biomol. Eng.* **2011**, *2*, 281–298.

(23) Lim, E.-K.; Jang, E.; Lee, K.; Haam, S.; Huh, Y.-M. *Pharmaceutics* **2013**, *5* (2), 294–317.

(24) Meng, F.; Cheng, R.; Deng, C.; Zhong, Z. *Mater. Today* **2012**, *15*, 436–442.

(25) Miller, M. A.; Zheng, Y.-R.; Gadde, S.; Pfirschke, C.; Zope, H.; Engblom, C.; Kohler, R. H.; Iwamoto, Y.; Yang, K. S.; Askevold, B.; Kolishetti, N.; Pittet, M.; Lippard, S. J.; Farokhzad, O. C.; Weissleder, R. *Nat. Commun.* **2015**, *6*, 8692.

(26) Pyonteck, S. M.; Akkari, L.; Schuhmacher, A. J.; Bowman, R. L.; Sevenich, L.; Quail, D. F.; Olson, O. C.; Quick, M. L.; Huse, J. T.; Teijeiro, V.; Setty, M.; Leslie, C. S.; Oei, Y.; Pedraza, A.; Zhang, J.; Brennan, C. W.; Sutton, J. C.; Holland, E. C.; Daniel, D.; Joyce, J. A. *Nat. Med.* **2013**, *19*, 1264–1272.

(27) Lapin, N. A.; Krzykawska-Serda, M.; Ware, M. J.; Curley, S. A.; Corr, S. J. *Cancer Nanotechnology* **2016**, DOI: 10.1186/s12645-016-0016-7.

(28) Naumenko, V.; Jenne, C.; Mahoney, D. J. *Methods Mol. Biol.* **2016**, *1458*, 217–230.